



Contents lists available at ScienceDirect

Fuel Processing Technology

journal homepage: www.elsevier.com/locate/fuproc

Development and validation of CFD models for gas phase reactions in biomass grate furnaces considering gas streak formation above the packed bed

Ali Shiehnejadhesar^{a,b,*}, Robert Scharler^{a,b,c}, Ramin Mehrabian^b, Ingwald Obernberger^{a,c}

^a Institute for Process and Particle Engineering, Graz University of Technology, Inffeldgasse 21b, 8010 Graz, Austria

^b BIOENERGY 2020 + GmbH, Inffeldgasse 21b, 8010 Graz, Austria

^c BIOS BIOENERGIESYSTEME GmbH, Inffeldgasse 21b, 8010 Graz, Austria

ARTICLE INFO

Article history:

Received 22 April 2015

Received in revised form 3 July 2015

Accepted 24 July 2015

Available online xxxxx

Keywords:

CFD modelling

Biomass

Combustion

Grate furnace

Streak formation model

Hybrid model

ABSTRACT

State-of-the-art packed bed models supply continuous concentration profiles as boundary conditions for subsequent CFD simulations of gas phase, leading to pre-mixed combustion conditions. However, in reality the “porous” nature of the packed bed leads to streak formation influencing gas mixing and combustion. Therefore, in the present work, in order to account for the influence of the streaks on gas phase combustion, a gas streak model based on a correlation between the local gas residence time and a mixing time has been developed based on numerical simulations. Finally, the streak model was linked with an in-house developed hybrid gas phase combustion model suitable for laminar to highly turbulent flow conditions and applied for an under-feed pellet stoker furnace (20 kW_{th}) concerning the simulation of gas phase combustion and NO_x formation. The results in comparison with a simulation without the streak formation model show that the flue gas species prediction can be improved with the proposed streak formation model. Especially, in the region above the fuel bed (in the primary combustion chamber), this is of special importance for NO_x reduction by primary measures.

© 2015 Elsevier B.V. All rights reserved.

1. Introduction and objectives

CFD modelling is becoming increasingly important for the development and optimisation of biomass grate furnaces. Here, gas phase combustion models play a key role concerning predictions of flow, temperature, and gaseous emissions (e.g. CO and NO_x).

The mode of gas combustion in a grate furnace can be classified as partially premixed with a locally differing mixing degree of oxidiser and fuel, whereas in this context the reactive gases released from the combusting biomass particles in the fuel bed are to be understood as (gaseous) fuel.

An empirical packed bed model developed by BIOS in cooperation with TU Graz [1–3] is usually being used at BIOENERGY 2020 + for the calculation of composition, temperature and velocity of the flue gas leaving the fuel bed. The empirical packed bed model, as most of the common packed bed models, calculates profiles of partially premixed flue gas compositions not considering spatial concentration gradients of oxygen and volatiles, since the fuel particles and the surrounding space cannot be resolved. However, in reality, the amount and distribution of combustibles and oxidiser in the gas released from the biomass

particles in the fuel bed are locally strongly differing, which is termed here as streak formation, influencing gas mixing and combustion.

Therefore, in this paper, a model which accounts for the influence of the streaks on gas phase mixing and reactions (e.g. combustion and NO_x formation) is introduced. The streak model is based on a correlation between the gas residence time and mixing time above the fuel bed, whereas the mixing time is defined as the necessary residence time to reach the fully mixed condition.

To derive the mixing time, a CFD case study with an ideally packed bed with spheres as fuel particles and non-reacting flow was performed to numerically derive the mixing time in dependence of relevant influencing parameters. The particle diameter was derived from the volume to surface area ratio of pellets according to EU standard [4,5]. The volatiles were represented by CO₂ released from the surface of the particles. The volatile release rate from a single particle was approximated with an in-house developed model [6] for single particle conversion. The influence of relevant parameters, like bed height, volatile mass flow rate and particle Reynolds number (calculated with the bulk flow velocity of primary air below the bed and the particle diameter), on mixing time was investigated.

In the next step, the model was linked with an in-house developed hybrid gas phase combustion model suitable for laminar as well as moderately to highly turbulent combustion conditions [7] and tested for a 20 kW_{th} under-feed pellet stoker furnace concerning the simulation of gas phase combustion and NO_x formation. The gas phase mixing and reaction progress is highly influenced by laminar and low turbulence

* Corresponding author at: Institute for Process and Particle Engineering, Graz University of Technology, Inffeldgasse 21b, 8010 Graz, Austria.

E-mail addresses: ali.shiehnejadhesar@gmail.com, ali.shiehnejad@bioenergy2020.eu (A. Shiehnejadhesar).

zones in the regions above the fuel bed and in small-scale biomass combustion applications in general. Therefore, the application of the hybrid model is relevant.

In order to highlight the advantages of the hybrid model and the streak formation model for the simulation of small-scale furnaces in terms of combustion and emission predictions, additional simulations were performed with different CFD gas phase reaction models like the eddy dissipation model (EDM) [8] and the eddy dissipation concept (EDC) [9]. All the simulations were performed with ANSYS® FLUENT® release 15.0. For the purpose of model evaluation, the simulation results were compared with CO and NO_x emission measurements.

2. Methodology

Firstly, an overview of the models applied for the case studies is given in the modelling section. Then, the non-reacting packed bed simulations for the derivation of the parameters of the streak formation model are described. Finally, the case study with the under-feed pellet stoker grate furnace for the test and evaluation of the streak formation model is introduced.

2.1. Modelling

In this chapter, the models used for the non-reacting packed bed simulations as well as the grate furnace simulations are explained. Then, the hybrid gas phase combustion model which is utilised for the grate furnace simulations is introduced. Finally, the streak formation model is presented.

2.1.1. Model overview

2.1.1.1. Case study with ideally packed bed. For the derivation of streak formation parameters, non-reacting multi-species simulations with an ideally packed bed with spheres have been performed. The SST $k-\omega$ low Reynolds turbulence model is applied to cover the whole range of flow conditions from laminar to turbulent flows in biomass grate furnaces. The primary air is injected uniformly below the fuel particles whereas the grate has been neglected. CO₂ is taken as trace species representing the volatiles release through the particle surface. To estimate the degree of mixing, a mixing state is defined (see Section 2.1.3). The mixing time is evaluated based on an estimated residence time to achieve a certain degree of mixing. The gas residence time is calculated by solving a scalar transport equation.

2.1.1.2. Furnace simulation. For the simulation of the under-feed stoker furnace, the following models have been applied: an empirical model developed by BIOS in cooperation with TU Graz [1–3] is used to describe the thermal decomposition of the solid biomass fuel. The model consists mainly of three parts. The definition of one-dimensional profiles along the grate concerning the degradation of the fuel components as well as fuel drying (part 1: based on assumptions and experimental data from test runs). In combination with the definition of conversion parameters (based on assumptions as well as experimental and literature data), which describe the formation of the most important flue gas components CH₄, CO, CO₂, H₂, H₂O, and O₂ as well as the NO_x precursors NH₃, HCN and NO (part 2), the stepwise balancing of mass and energy fluxes released from the fuel bed is possible (part 3) [1–3]. The calculation results are used as boundary profiles for subsequent CFD simulations of the reactive flow in the furnace.

The EDM, the EDC and hybrid gas phase reaction models were used for the simulations of turbulent reactive flow in the combustion chamber. The solution of the EDM simulation, which is specially adapted for biomass grate furnaces with a global 3-step reaction mechanism [1,10,11], was used as starting solution for the subsequent EDC and hybrid model simulations. In the case of the hybrid model, an additional simulation was performed by taking into account the effect of streak

formation. The latter will be referred to as hybrid-streak model throughout the paper.

The In-Situ Adaptive Tabulation (ISAT) algorithm by Pope [12] has been used to speed-up the CPU-intensive treatment of the detailed reaction kinetics for the EDC, hybrid and hybrid-streak simulations. The discrete ordinate model (DOM) model was applied to simulate radiative heat transfer in the furnace. A domain based weighted-sum of gray-gases model (WSGGM) was used to calculate the absorption coefficient of the gas phase. Since the temperature and flue gas species specified by the empirical packed bed model are fixed at the surface of the fuel bed, there is no feedback from the freeboard on the bed model. The Realizable $k-\epsilon$ turbulence model was used for turbulence. Together with the Realizable $k-\epsilon$ model, the enhanced wall treatment model is used, which is a two-layer turbulence approach combined with enhanced wall functions [13]. The model is valid throughout the near-wall region (i.e., laminar sub-layer, buffer region, and fully-turbulent outer region). Therefore, the model is supposed to be valid for low and high Reynolds wall-bounded flows. It should be noted that the SST $k-\omega$ low Reynolds turbulence model was applied as suitable turbulence model above the packed bed to predict the mixing time since the flow is weakly turbulent. In the furnace simulation, the mixing delay due to the streaks, which is assumed to be dominating over the turbulent mixing above the bed, is considered with the streak model. Moreover, the Realizable $k-\epsilon$ model gives considerably better results concerning the mixing of round jets in gas streams [1,14] than the SST $k-\omega$ model. The governing equations consist of incompressible Favre-averaged transport equations of continuity, momentum, energy, radiation, turbulence and species conservation equations. A second-order upwind discretisation scheme was used to solve all governing equations. Mass diffusion coefficients are required whenever species transport equations in multi-component flows are solved. The constant dilute approximation method with a value of 2.88×10^{-5} was used for the diffusion coefficient of each species in the mixture. An overview of the solution algorithm used for the furnace simulations with different gas phase reaction models is shown in Fig. 1. Under the assumption that NO_x formation reactions do not significantly influence the flow pattern in the furnace, a time saving 2-step approach is applied for CFD simulations. The basic gas phase combustion simulation has been performed using the EDC, hybrid and hybrid-streak combustion models with the C—H—O subset of the Skeletal Kilpinen97 mechanism (12 species and 25 reactions) [15], which has extensively been validated for grate furnaces [15]. The subsequent CFD simulation of gas phase fuel NO_x formation in a post-processing mode has been done using the EDC, hybrid and hybrid-streak models in combination with a detailed reaction mechanism (28 species and 102 reactions in total) [15]. Here, it is worth to mention that, the EDM in combination with global reaction mechanisms is not able to describe complex interactions of turbulence and multi-step reaction kinetics as given in the case of NO_x formation in biomass combustion plants. Therefore, the NO_x simulations reported in this paper were only performed with the EDC, the hybrid and the hybrid-streak model.

2.1.2. Hybrid gas phase reaction model

2.1.2.1. Bulk flow. An in-house developed hybrid gas phase reaction model, suitable for laminar to highly turbulent flows, has been applied for the simulation of the reacting gas flow. In particular, in the region above the fuel bed and in small-scale biomass combustion plants, gas phase mixing is highly influenced by laminar and low turbulence zones. Here, the eddy break-up combustion models are not valid because they were originally developed for highly turbulent flows. Therefore, a hybrid eddy dissipation concept (EDC)/finite rate kinetics model (FRK) has been developed, which calculates the effective reaction rate from laminar finite rate kinetics and the turbulent reaction rate and weights them depending on the local turbulent Reynolds number of the flow.

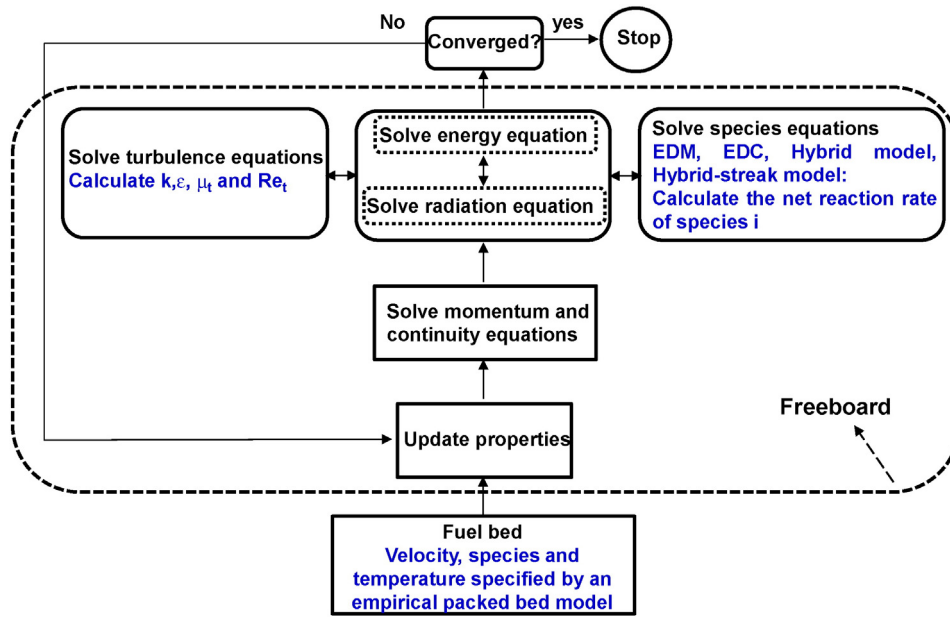


Fig. 1. Overview of the solution algorithm.

For a multi-component system, the species mass conservation equation is defined as follows;

$$\frac{\partial}{\partial t}(\rho Y_i) + \nabla \cdot (\rho \vec{v} Y_i) = -\nabla \cdot \vec{J}_i + R_i \quad (1)$$

where ρ is the mixture density, Y_i is the mass fraction of species i , \vec{v} is the velocity vector, \vec{J}_i is the diffusion flux of species i due to concentration gradients, and R_i is the net rate of production of species i by chemical reactions.

In the hybrid model, the mean chemical reaction (second term in the right hand side of Eq. (1)) is modelled as:

$$(R_i)_{\text{Hybrid}} = \left(\frac{2}{1 + Re_t}\right)(R_i)_{\text{FRK}} + \left(\frac{Re_t - 1}{1 + Re_t}\right)(R_i)_{\text{EDC}} \quad (2)$$

where $(R_i)_{\text{FRK}}$ is the FRK mean reaction rate, the term $(R_i)_{\text{EDC}}$ is the mean reaction rate calculated by the EDC model and Re_t is the turbulent Reynolds number which is defined as follows:

$$Re_t = \frac{\rho k^2}{\nu \varepsilon} \quad (3)$$

In the laminar range, the reaction rate is calculated with pure finite rate kinetics and in the highly turbulent region with the EDC. In the transition region around $Re_t = 64$, the overall reaction rate is calculated as the sum of the weighted reaction rates of finite rate kinetics and the EDC. In other words, the overall reaction rate is determined as a linear combination of the two reaction rates. The hybrid model has been extensively validated for a series of diffusion jet flames covering laminar, transitional, and turbulent flow conditions. A detail description of the hybrid gas phase reaction model can be found in [7].

2.1.2.2. Near-wall combustion. In the hybrid gas phase reaction model, the overall reaction rate is calculated by a weighted reaction rate. The hybrid model gives results which are close to the FRK model when approaching the laminar regime, while the results are close to the EDC in the high turbulence region. The weighting factors in the hybrid model are a function of the turbulent Reynolds number of the flow. This imposes problems in the near wall region, when the flow cannot be sufficiently resolved, which is true in most of the real-scale combustion

applications with wall-bounded flows involved. One challenge in CFD is how to treat the thin near-wall sublayer, where viscous effects are important. Generally, in turbulent wall flows, two distinct zones exist near the wall. Firstly, the viscous sublayer which is completely dominated by viscous effects. The so-called “outer region” shows a nearly constant velocity with distance from the wall. Fig. 2 (left) shows the distinct areas existing near the wall in turbulent wall flows. A non-dimensional wall distance (y^+) is used to differentiate the regions that exist near the wall. The y^+ can be interpreted as a local Reynolds number with the wall distance as length scale, so its magnitude defines also the relative importance of viscous and turbulent processes [16]. To support this hypothesis, Fig. 2 (right) shows the fractional contributions of viscous and Reynolds stresses to the total stress in the near-wall region of a channel flow taken from [16,17]. When the stresses are plotted against y^+ , the profiles depicted for two Reynolds numbers almost collapse. The viscous contribution drops from 100% at the wall ($y^+ = 0$) to 50% at $y^+ = 12$ and is less than 10 at $y^+ = 50$.

Therefore, an accurate resolution of this layer can be crucial. This is due to the steep gradient of the mean values (e.g. transport of mean momentum and other parameters) that occur in the boundary layer. There are two approaches to model the near-wall-region. The most reliable way is to use modified turbulence models (e.g. low-Re-number turbulence models) to resolve viscosity-affected region (i.e. near wall regions) with a mesh which is fine enough to resolve the steep gradients near the wall, including the viscous sublayer. However, this can be very computationally expensive, particularly in 3D cases. Hence, the traditional industrial solution is to use wall-functions for flow modelling. Enhanced wall treatment is a near-wall modelling method that combines a two-layer model (i.e. linear (laminar) and logarithmic (turbulent)) with enhanced wall functions. The method formulates the law-of-the-wall as a single wall law for the entire wall region. ANSYS® FLUENT® achieves this by blending the linear (laminar) and logarithmic (turbulent) laws-of-the-wall using a function suggested by Kader [13] as follows:

$$u^+ = e^{\Gamma} u_{\text{laminar}}^+ + e^{1-\Gamma} u_{\text{turbulent}}^+ \quad (4)$$

where Γ is a blending function in dependence of y^+ and is given by:

$$\Gamma = -\frac{0.01(y^+)^4}{1 + 5y^+} \quad (5)$$

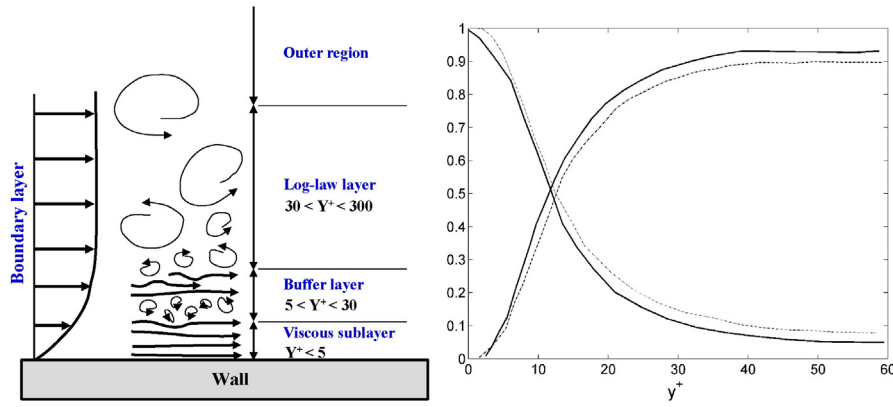


Fig. 2. Areas of turbulent wall flows (left) and fractional contributions of viscous and Reynolds stresses to total stress in the near-wall region of a channel flow (right) (adapted from Chapter 7 in [16]) taken from [17] (dashed lines, $Re = 5600$; solid lines, $Re = 13,750$).

where $u^+_{laminar}$ and $u^+_{turbulent}$ are the dimensionless velocities. The definitions of y^+ , $u^+_{laminar}$ and $u^+_{turbulent}$ can be found in [16]. Fig. 3 shows the trend of the blending factors in dependence of the non-dimensional wall distance (y^+). This formula also guarantees the correct asymptotic behaviour for large and small values of y^+ and reasonable representation of velocity profiles in the cases where y^+ falls inside the wall buffer layer.

In the hybrid combustion model, close to the wall, the turbulent Reynolds number of the flow approaches zero and the reaction rate is mainly calculated by the FRK model, despite the fact that the larger fraction of the flow in the wall near cell is influenced by inertial forces (Reynolds stresses). In conclusion, in reacting flows, it is also a problem of not sufficiently resolving the wall, which leads to the consideration of flow regime when calculating the reacting rate, while in reality there is a rapid change of the flow regimes in the boundary layer. To avoid this, the reaction rate has to be weighted in dependence of the flow regime inside the wall cell. Therefore, the mean chemical reaction rate for the near wall cells can be adjusted by blending the FRK and EDC models using a function suggested by Kader [13] as follows:

$$(R_i)_{wall} = e^\Gamma (R_i)_{FRK} + e^{1-\Gamma} (R_i)_{EDC} \quad (6)$$

where Γ is a blending function as defined in Eq. (5). The usage of y^+ in the blending function represents the concept of local Reynolds number of the flow as earlier explained [16]. In this formulation, the FRK and the EDC are weighted according to the fractional contributions of the

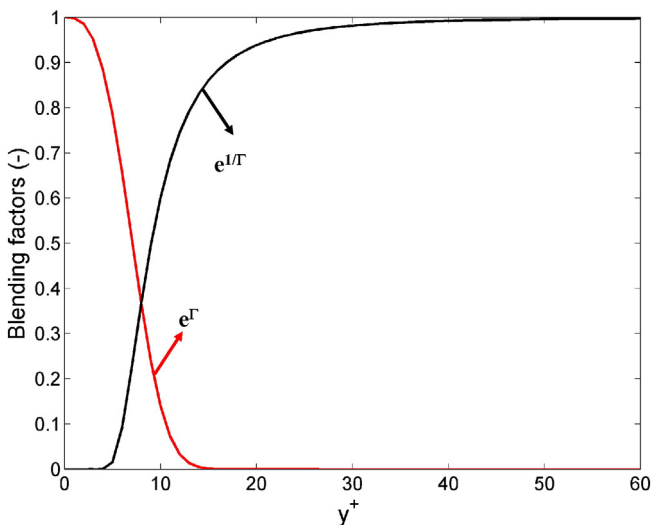


Fig. 3. Trend of blending factors in dependence of y^+ .

viscous and Reynolds stresses in the near-wall region and the overall reaction rate in the wall cell is calculated as the sum of the weighted reaction rates of the FRK and the EDC. As shown in Fig. 3, in the laminar range ($y^+ < 5$) the reaction rate is calculated with pure finite rate kinetics and in the turbulent region ($y^+ > 30$) with the EDC. In the transition region around $y^+ = 10$ (i.e. buffer layer), the contribution of viscous and Reynolds stresses is interchanging. Therefore, the overall reaction rate in the wall cell is calculated by a combination of the two terms. Hence, the overall reaction rate is weighted by two terms as a function of y^+ .

This near wall combustion approach was implemented in the hybrid model. The cases that have been simulated with the hybrid and the hybrid-streak model in this paper utilise the near wall combustion approach embedded in the hybrid model.

2.1.3. Streak formation model

A streak formation model has been developed. The model is based on a mixing time, where the gas streaks arising from the fuel bed are fully mixed, and a correlation with the residence time of the flue gas released from the fuel bed. In order to describe the mixing process above the packed bed, a criterion has been defined to calculate the mixing state (MS) as follows:

$$MS = 1 - \frac{C_{fm} - C(t)}{C_{fm}} \quad (7)$$

Here, C_{fm} is the tracer gas concentration (here CO_2) in the fully mixed gas and $C(t)$ is the local tracer gas (CO_2) concentration in dependence of the mixing time. The residence time which is necessary to reach the defined mixing state (here, $0.99 < MS < 1.01$ has been defined) is the mixing time t_{fm} . Finally, the mixing function (MF) is the combination of the mixing time t_{fm} and the gas residence time t_{gas} :

$$MF = \min\left(\frac{t_{gas}}{t_{fm}}, 1\right) \quad (8)$$

where

- MF = 0 (completely unmixed)
- MF = 1 (completely mixed).

The mixing function provides information about the mixing quality of the volatiles and the primary air, it varies between 0 (no mixing) and 1 (fully mixed). The mixing time (t_{fm}) is derived from the packed bed case studies and is a constant value. Therefore, Eq. (8) can be considered as a linear correlation of t_{gas} which is bounded between 0 and 1.

A user-defined scalar approach (UDS) is used to calculate the gas residence time inside the combustion unit. The approach proved to be

valid for use in modelling heating, ventilation, air conditioning and hydraulic systems [18,19].

For an arbitrary scalar, φ_k (here gas residence time), the steady state transport equation to be solved is given by [18,19]:

$$\frac{\partial}{\partial x_i} \left(\rho u_i \varphi_k - \Gamma_k \frac{\partial \varphi_k}{\partial x_i} \right) = S_{\varphi_k} \quad (9)$$

where, Γ_k is the diffusion coefficient and S_{φ_k} is the source term.

The diffusivity of the UDS is defined to be the same as of the flue gas since the residence time is transported and mixed with the gas flow. Therefore, in turbulent combustion flows, the diffusivity of the UDS is a function of the binary diffusivity, the turbulent and laminar viscosities, and the turbulent Schmidt number and is defined as follows [19]:

$$\Gamma_k = D_b \rho + \frac{\mu_l + \mu_t}{Sc_t} \quad (10)$$

where, ρ is the density of the flue gas, D_b is the binary diffusivity of the flue gas (with a value of 2.88×10^{-5} which is also applied for the diffusion coefficient of each species in the mixture), μ_l and μ_t are the laminar and turbulent viscosities of the flue gas and Sc_t is the turbulent Schmidt number (with a value of 0.7 which is also applied for the species transport equation) defined as:

$$Sc_t = \frac{\mu_t}{\rho D_t} \quad (11)$$

where D_t is the turbulent diffusivity of the flue gas. The effect of turbulence fluctuations is taken into account in the calculation of residence time implicitly since the effect of turbulent viscosity is considered in the diffusivity of the scalar transport equation.

At time t the mass flow rate of a fluid into a cell is m^* , therefore, the value of the scalar when it enters the cell is m^*t . When the fluid leaves the cell, its age is increased by Δt , therefore, the value of the scalar when it leaves the cell is $m^*(t + \Delta t)$. In order to find the time at which the fluid leaves, a source term is required equivalent to:

$$S_{\varphi_k} = \frac{m^* \Delta t}{V} \quad (12)$$

where, m^* is the mass flow rate and V is the volume of the computational cell.

The source term is divided by the cell volume since it is applied on a volumetric basis. Since neither the time nor the mass flow rate through the cell is known, the following relationship could be applied to simplify the source term:

$$m^* = \rho A u = \rho V' \quad (13)$$

where A is the area of the cell and V' is the volumetric flow rate.

By rearranging Eq. (13) we have

$$V' = \frac{m^*}{\rho} \quad (14)$$

and since

$$\Delta t = \frac{V}{V'} \quad (15)$$

by substituting Eq. (14) into Eq. (15) we have

$$\Delta t = \frac{V \rho}{m^*} \quad (16)$$

Now, by substituting Eq. (16) into Eq. (12), the source term can be found as follows:

$$S_{\varphi_k} = \rho. \quad (17)$$

A second-order upwind discretisation scheme was used to solve Eq. (9). Eq. (9) has been implemented by a user-defined function (UDF) in ANSYS® FLUENT®.

Finally, the effective reaction rate is calculated by multiplying the mixing function, which defines the macro-mixing state, with the reaction rate, calculated by the hybrid combustion model as follows:

$$(R_i)_{\text{Hybrid-streak}} = MF \times (R_i)_{\text{Hybrid}} \quad (18)$$

Therefore, at positions where mixing is poor the rates of homogeneous reactions are damped which leads to streaks above the bed. The term “streaks” is used to represent the definition of the mixing function.

2.2. Case study for the derivation of the streak formation model

A CFD study with an ideally packed bed with spheres as fuel particles and non-reacting flow has been performed in order to numerically derive the mixing time. The volatiles were represented by CO_2 released from the surface of the particles in the bed. The volatile release rate from single particles was approximated by an in-house developed layer model [6] for the conversion of thermally thick biomass particles. In this parameter study, the following influencing parameters have been investigated for a packed bed: bed height, volatile mass flow rate and bulk flow velocity of primary air below the bed. The bed height was varied by particle layers from 5 to 15 layers. During typical biomass combustion conditions with air staging the most relevant components released are H_2O , CO_2 , CO , H_2 and CH_4 [20–22]. However, during packed bed combustion, the dominant gas volume flux is from the primary air passing through the packed bed. In CFD simulations the density of the mixture is usually considered as incompressible ideal-gas (due to the low pressure changes) and mainly depends on the temperature inside the combustion chamber that influences the volume flow rate of the volatiles released from the biomass particles. Furthermore, to qualify the effect of mixing between primary air and volatiles the volatile composition plays no role, while the released volume flow (which depends on temperature) is important. Moreover, since a non-reacting simulation is performed, for the release rates only an average value can be estimated. Therefore, a sensitivity analysis concerning the influence of the volatile release rate was performed. In order to cover the possible range of released volume fluxes, the estimated value of the reference case was multiplied by a factor x . A typical volatile release rate was estimated with the layer model; for the investigation of the sensitivity of the results on the release rates, this value has been varied between a factor of 1 to 1.7. It could be shown that the influence of the release rate is comparably low.

Bulk flow velocity of primary air below the bed was varied between 0.1 and 7 (m s^{-1}). In biomass grate furnaces, the flow above the fuel bed is typically in the low Re range. Usually, the primary air velocity fed below the grate may vary between 0.1 and 7 (m s^{-1}). The values are gained from an in-house developed empirical packed bed model [1–3]. Therefore, to cover all ranges of flow conditions for small to large-scale biomass combustion plants, a sensitivity analysis has been performed.

The diameter of the spheres was approximated based on the volume to surface area ratio of pellets according to the respective EU standard [4,5]. As mentioned, the study has been performed for pellets as fuel. However, the simulation results can be applied for all particle sizes by applying the particle Reynolds number for the look-up table where the results are summarised. Here, three parameter studies with an ideally packed bed with the different bed heights and number of particle layers, respectively, were performed in order to calculate the mixing

time in dependence of the influencing parameters. Fig. 4 shows the CFD domain of the packed bed for 5 layers considered in this study. An unstructured computational grid with 2, 4 and 6 million cells in total was used for the simulation of the packed bed with 5, 10 and 15 numbers of layers, respectively. On the surface of the particles, a number of layers with prismatic grid (10 layers) are used to resolve the viscous sublayer. It has been assured that the first grid point (the thickness of the first layer of the prismatic cells was about 0.007 mm) is located in the viscous sublayer ($y^+ < 1$). The primary air was injected below the bed with an even distribution and the volatiles represented by CO_2 as tracer gas were released from the surface of the spheres. Moreover, different planes above the bed were defined to evaluate the mixing state and mixing time. In the definition of the packed bed, the reference plane and the other planes above it are fixed at a certain height for each number of layers studied. This means that all the layers are arranged below the reference plane (see also Fig. 4).

A simulation matrix was built for each layer to derive the mixing time based on the primary air velocity and volatile mass flow rate. The flow simulation was performed for all primary air velocities and volatile mass flow rates. Then, the mixing state was calculated at each plane defined above the bed. Finally, the mixing time was derived based on the estimated gas residence time which is necessary to reach the defined mixing state (here, $0.99 < MS < 1.01$).

Therefore, the mixing time can be represented by influencing parameters like primary air velocity and number of layers considered in the simulations. To make the model applicable for all fuel particle sizes, the mixing time can be represented as function of the particle Reynolds number instead of the primary air velocity. The particle Reynolds number can be defined as follows:

$$\text{Re}_p = \frac{V_{\text{primary air}} d_v}{\nu_{\text{air}}} \quad (19)$$

where $V_{\text{primary air}}$ is the primary air released below the particles, ν_{air} is the air kinematic viscosity and d_v is the volume diameter.

The volume diameter d_v [23] can be derived based on the diameter of a sphere having the same volume as the biomass particles. The biomass particle volume can be estimated from the average size of the biomass particles.

2.3. Test and verification of the streak formation model for small-scale biomass under-feed stoker furnaces

To investigate and verify the influence of the streak formation model on gas phase mixing and reactions, a CFD simulation was performed for an under-feed stoker furnace (20 kW_{th}).

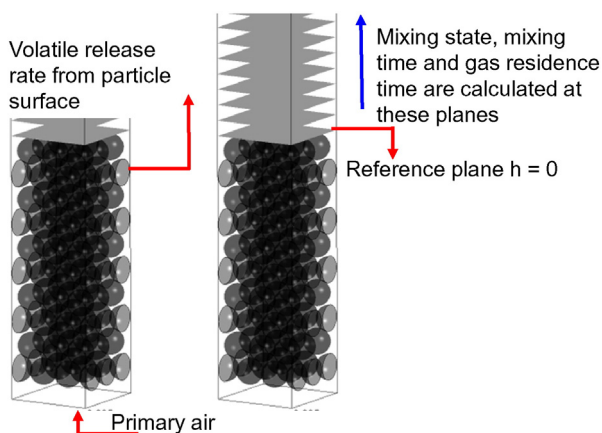


Fig. 4. CFD domain and boundary conditions for the evaluation of the mixing time above a packed bed.

The under-feed stoker furnace used for the test of the streak formation model is shown in Fig. 5. The simulation domain comprises the combustion chamber above the fuel bed till the exit of the hot water fire tube boiler. For the furnace simulation, an unstructured computational grid with 2 million cells in total was used while 7 layers are used with prismatic grid with initial prism height of 2 mm to resolve the viscous sublayer. It is necessary to resolve the viscous sublayer for small-scale plants since the low Reynolds regions are of high relevance. However, in larger plants the flow is fully turbulent and it is not economic to resolve the viscous sublayer due to high computational costs. The fuel is fed on the grate from below and is transported towards the outer edge of the grate. Primary air is supplied through the grate by nozzles at the bottom which form a concentric ring with the fuel feeding tube in the centre. The secondary air is injected through the secondary air inlet channel and is distributed in annular space of secondary air supply (see Fig. 6). There are twelve secondary air nozzles located on the circumference of the burner. However, every third nozzle is blocked and only eight nozzles are open in this case study. The secondary combustion zone is located after the secondary air is introduced. Moreover, there is no flue gas recirculation considered in this case study. Moreover, false air supply into the combustion chamber due to the ash removal system is considered. A certain amount of leakage air (10% of primary air), obtained from measurements during test runs, was taken into account in the simulation as false air.

The water side of the fire tube boiler walls was not included in the simulation. A convection boundary condition with 75 °C (average water temperature) and a typical heat transfer coefficient for water in forced convection (2000 W/m² K) are used as framework conditions for the fire tube boiler walls.

The simulations were performed for two biomass fuels, wood pellets and straw pellets, for which the experimental data concerning CO and NO_x emissions were available. Table 1 provides the most relevant operating conditions of the furnace and fuel composition.

3. Discussion of the results

3.1. Derivations of the streak formation model constants

An initial case study was performed to investigate the effect of the number of layers (bed height) on mixing. Fig. 7 shows the mixing state (Eq. (7)) variations in dependence of bed height for different numbers of layers. In the parametric case studies, the mixing state is calculated as a scalar field variable and evaluated in several planes defined above the packed bed. One can evaluate for each plane the maximum or minimum value of the tracer gas concentration for the definition of

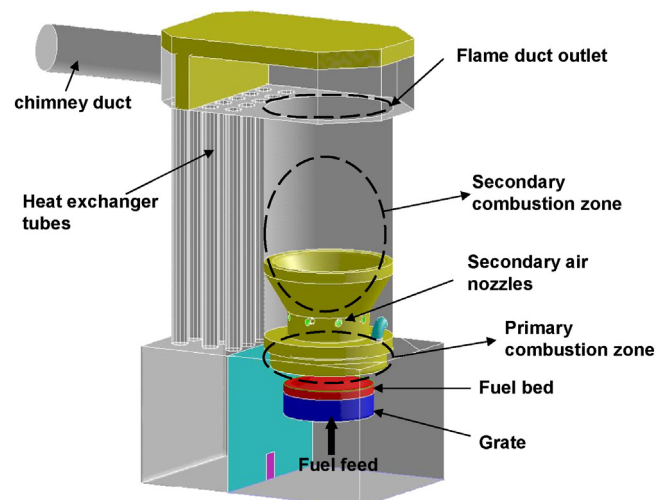


Fig. 5. Geometry of the under-feed stoker furnace with a fire-tube hot water boiler.

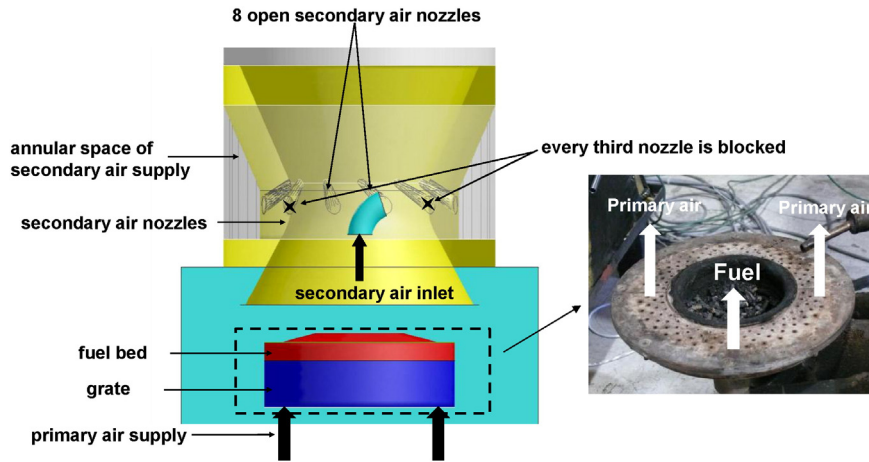


Fig. 6. Close-up of the primary and secondary air supplies.

the mixing state. In the present study, the maximum value of the mixing state is determined at each plane. By doing this, the mixing state is derived in dependence of the height above the bed.

The results show a strong effect of the number of layers (bed height) on mixing. Hence, it was considered as an independent parameter. Afterwards, a simulation matrix was defined in order to investigate the effect of primary air velocity and volatile mass flow rate variations on the mixing (mixing state) for each number of particle layers defined (5, 10 and 15 layers).

Fig. 8 shows the mixing state in dependence of bed height for different volatile mass flow rate variations at two selected primary air velocities and under consideration of 10 layers. The results confirm that the effect of volatiles is insignificant on the mixing in comparison to the effect of primary air mass flow rate since the fraction of the volatile release rate to the primary air is low (e.g. 0.1–0.3). Because the mass flow of volatiles compared to the primary air mass flow is low and hence was expected to have an insignificant effect on mixing in comparison to the primary air flow rate, a value considerably higher than the reference value was investigated first. Since it showed nearly no difference to the results with the reference value, a reduction of the amount of flue gas below the reference value was expected to have even less effect and it was thus not investigated.

The effect of primary air velocity variations on the mixing state for different numbers of layers (10 and 15 layers) is shown in Fig. 9. The results in Fig. 9 are shown in dependence of particle Reynolds number instead of velocity. The results indicate that the mixing state strongly

depends on the particle Reynolds number and, therefore, primary air velocity. The change of the slope in Fig. 9 in the range of 15–20 mm could be explained by a change in the flow regime from laminar to turbulent conditions (i.e. transition regime) in the range between $Re_p = 237\text{--}947$ (–) (i.e. the primary air velocity is in the range between 0.7 and 1 m s^{-1}). Hence, the length of the streaks in dependence of particle Reynolds number (defined by the criterion for fully mixed conditions) is oscillating in this range. As already explained, the mixing function is a linear correlation between the mixing time and the gas residence time. The mixing time is a constant, which is a value of the gas residence time at fully mixed conditions ($MS = 1$). Since the mixing state as a function of the height above the bed shows an asymptotic behaviour (fully mixed conditions with $MS = 1$ will never be reached) a certain tolerance has to be defined to achieve the mixing time. The tolerance has to be in a certain range in order to minimise its influence. Therefore, on the one hand the value of the mixing state (for fully mixed conditions) has to be close to one. On the other hand (as can be seen in Fig. 9) it should be on the branch of an individual curve with a rapid change of the mixing state, since on the flat branch the mixing time and hence the mixing function strongly changes when varying the tolerance and hence the mixing state. The evaluation of mixing time (t_{fm}) was done based on a certain error tolerance (here 1%) since the mixing state has asymptotic behaviour that means it never reaches the perfect mixing condition (i.e. $MS = 1$). The red line in Fig. 9 represents the error tolerance used to derive the mixing time. It has been

Table 1
Operating conditions and fuel characteristics of the furnace.

Operating conditions	Unit	Wood pellets	Straw pellets
Nominal boiler load	kW	21	19
Adiabatic flame temperature	°C	1501	1360
Flue gas recirculation ratio	–	0	0
λ_{prim}	–	0.64	0.69
λ_{total}	–	1.58	1.71
Fuel composition	Unit	Wood pellets	Straw pellets
Ash	Mass fraction d.b.	0.40	7.30
C	Mass fraction d.b.	50.10	46.10
H	Mass fraction d.b.	5.70	5.80
O	Mass fraction d.b.	43.77	40.20
N	Mass fraction d.b.	0.07	0.54
S	Mass fraction d.b.	0.0	0.17
Moisture content	Mass fraction w.b.	8.10	8.10
GCV	MJ/kg d.b.	20.24	18.56
NCV	MJ/kg w.b.	17.24	15.69

Explanations: w.b.: wet basis; d.b.: dry basis; GCV: gross calorific value; NCV: net calorific value; λ_{prim} : primary air ratio related to primary air supplied below the grate including the false air; λ_{total} : total air ratio related to total amount of air supplied.

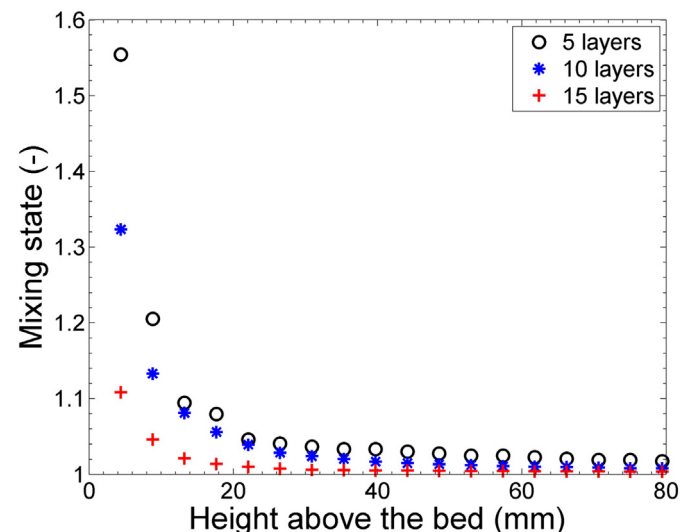


Fig. 7. Maximum mixing state above the bed (–) evaluated for different numbers of layers.

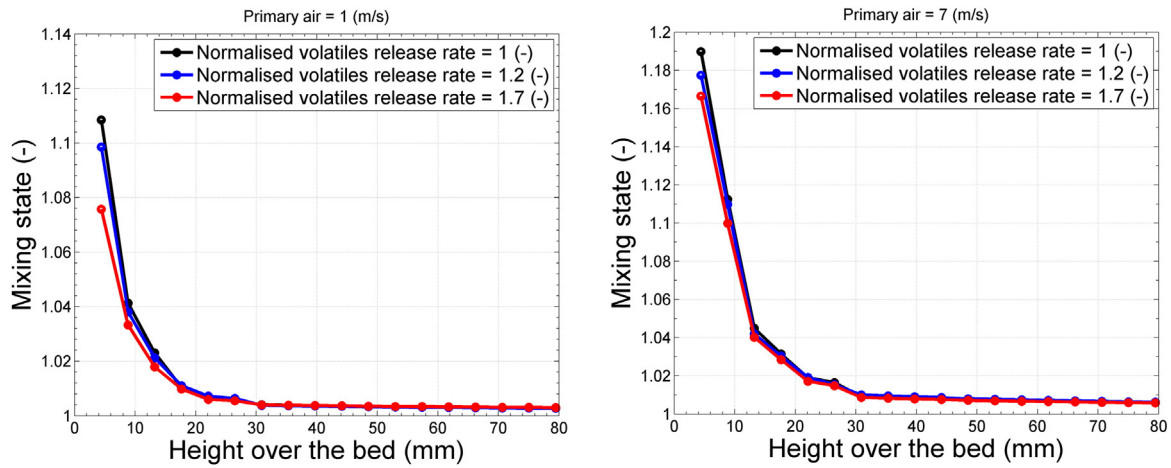


Fig. 8. Maximum mixing state (-) evaluated for different volatile release rates for 10 layers (left: primary air velocity 1 (m s⁻¹), right: primary air velocity 7 (m s⁻¹)).

confirmed that 1% error tolerance is fine enough for all cases considered to derive the mixing time.

Fig. 10 shows the mixing time behaviour in dependence of the particle Reynolds number as well as the number of layers. For all layers considered, a trend concerning the mixing time in dependence of the particle Reynolds number was found. The non-monotonic behaviour in Fig. 10 could also be explained by a change in flow regime from laminar to turbulent conditions (i.e. the transition regime) (see Fig. 9). Hence, the length of the streaks in dependence of particle Reynolds number (defined by the criterion for fully mixed conditions) is oscillating in this range. The results showed that the mixing time of the streaks increases as the particle Reynolds number increases. Generally, at lower particle Reynolds numbers the mixing time is lower. This attributes to a higher residence time of the flue gas due to lower primary air velocities

which results in a shorter streak length above the packed bed. The mixing time increases as the particle Reynolds number (i.e. primary air velocity) rises due to a higher streak length above the packed bed. Moreover, the mixing time for all particle Reynolds numbers is lower for a larger packed bed height since a higher residence time inside the packed bed improves mixing of primary air and volatile matter. The results of this case study serve as look-up table for the calculation of the mixing time in dependence of the different influencing parameters. For practical application (e.g. the furnace simulation with the streak formation model – see Section 3.2) the mixing time (t_{fm}) can be retrieved by a linear interpolation between the calculation points through an estimation of the particle Reynolds number and the number of layers. The particle Reynolds number can be easily calculated from the velocity profile specified by the empirical packed bed model along the grate and the

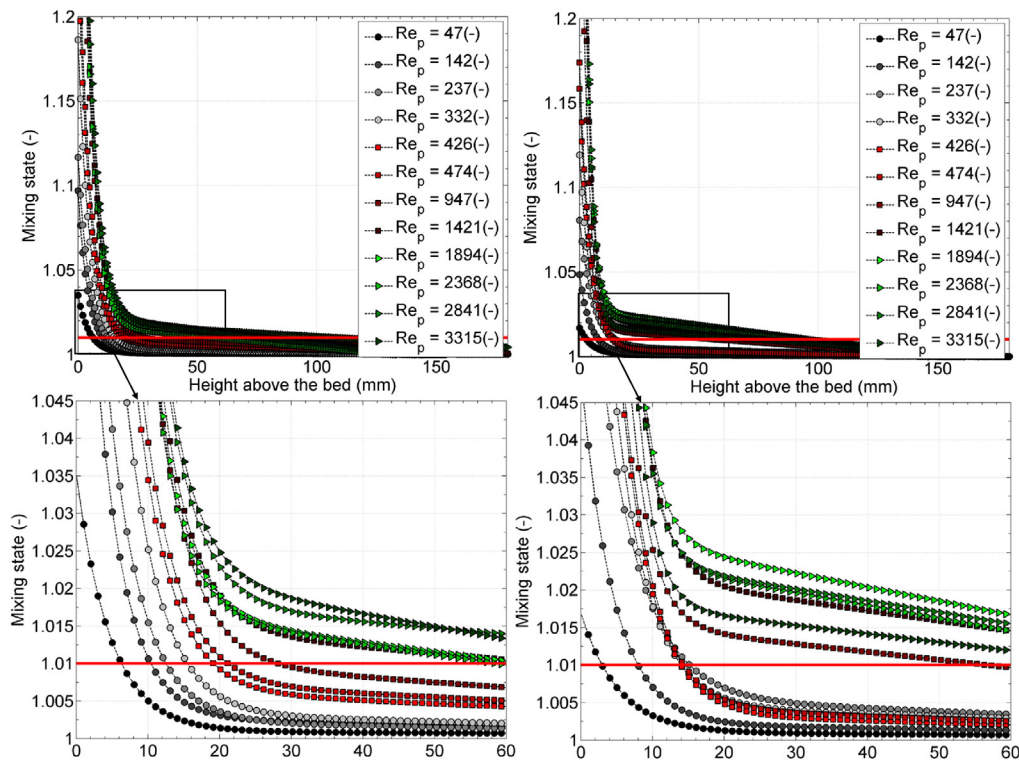


Fig. 9. Maximum mixing state (-) evaluated for different particle Reynolds numbers (left: 10 layers, right: 15 layers). (For interpretation of the references to colour in the text, the reader is referred to the web version of this article.)

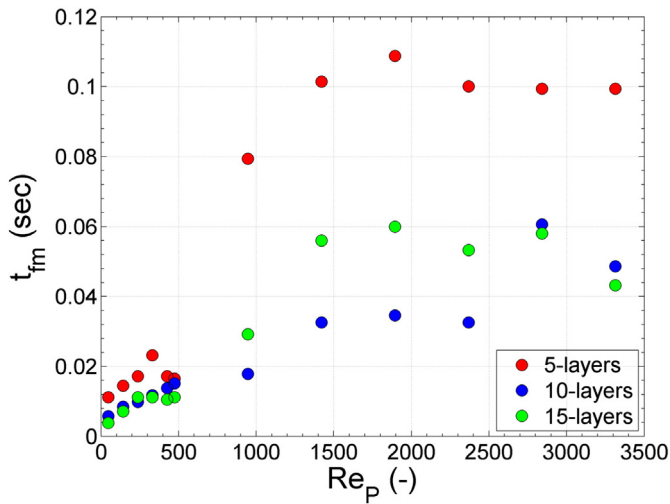


Fig. 10. Mixing time (s) for different particle Reynolds numbers and different numbers of particles.

average particle diameter (e.g. volume diameter [23]). Also, the number of layers can be estimated by the initial estimated height of the packed bed and the diameter of the fresh biomass fuel fed. The number of layers represents the number of particles that can be stacked in that length (e.g. length divided by the diameter of particles). Since the total number of particles on the bed remains constant on average for a certain operating condition, also the number of layers remains constant over the grate length.

3.2. Test of the steak formation model for a biomass under-feed stoker furnace

In this section, the results for the simulation of the 20 kW biomass under-feed stoker furnace are shown. The mixing function needs to be evaluated for the present case to investigate the effect of the streak formation model on the combustion simulation. Therefore, the mixing function evaluation is presented for the case wood pellets. However, the same approach was applied to derive the mixing function for straw pellets (not shown here). Fig. 11 (left) shows the calculated particle Reynolds number as well as the number of layers along the grate for wood pellets as fuel. The particle Reynolds number was calculated based on the velocity profile calculated with the empirical packed bed model (the maximum primary air velocity was about $2.5 \text{ [m s}^{-1}]$ in the present case). The particle diameter was estimated from the volume

diameter (see Section 2.2) (the wood pellet particles were assumed as spheres with a $d_v = 6 \text{ [mm]}$). The number of layers can be estimated by the initially estimated height of the packed bed and the diameter of the fresh wood pellets fed. The kinematic viscosity of the flue gas was taken from the CFD simulation results stored in the centre of the cells along the grate surface. A tetrahedral mesh was applied, which results in different distances from the grate surface (boundary of the simulation domain). Since the temperature profile values calculated with the empirical packed bed model and applied as boundary condition of the CFD simulation are not the same as the gas temperatures stored in the centre of the adjacent cells, the varying cell centre distances from the surface of the grate causes fluctuations in gas temperature and, therefore, of the viscosity as a function of the gas temperature. Therefore, the particle Reynolds number profile shows disturbances (Fig. 11 (left)). To derive a mixing time profile along the grate (Fig. 11 (right)) the values were retrieved from the look-up table for the mixing time (as described in Section 3.1). In the present case the mixing time could also be simplified by a constant value. But since using release profiles with varying influencing parameters on the mixing time, the range of the mixing time is not known in advance. Therefore, a method is needed for the calculation of mixing time profiles. Hence, the profile of the mixing time is used as an initial boundary condition at the surface of the fuel bed. Then a transport equation is solved to obtain the mixing time as a field variable in the CFD domain. Therefore, the mixing time has a higher relevance in comparison to the initial conditions.

The shrinkage of the particles along the grate is implicitly considered in the simulations since the shape of the fuel bed and the path of particles along the grate is assumed based on visual observation. Furthermore, it is assumed, that the number of particles (i.e. 5) and the horizontal velocity on the grate remain constant along the grate, since the initial values of mass flux, particle size and particle density are held constant, and moreover, the entrainment of particles from the grate and the fragmentation of the particles are neglected. With the information of the locally assumed bed height and the initial values of particle density, porosity and particle mass flux, the local particle volume and shrinkage respectively, can be estimated (the diameter change is thus implicitly considered).

Finally, two transport equations were solved, one for the gas residence time and the other for the mixing time, to derive the local mixing function defined in Eq. (8). Fig. 12 shows the contour plots of gas residence time (left) and the mixing function (right) derived from Eq. (8).

Finally, the mixing function defined is linked with the hybrid combustion model. The mixing function indicates that a major part of the reaction zone above the packed bed is influenced by streak formation. The mixing function as defined shows the degree of mixing above the grate. The value 0 means no mixing and 1 means fully mixed. As can be seen from Fig. 12 (right), the mixing function varies between 0 and 1. The

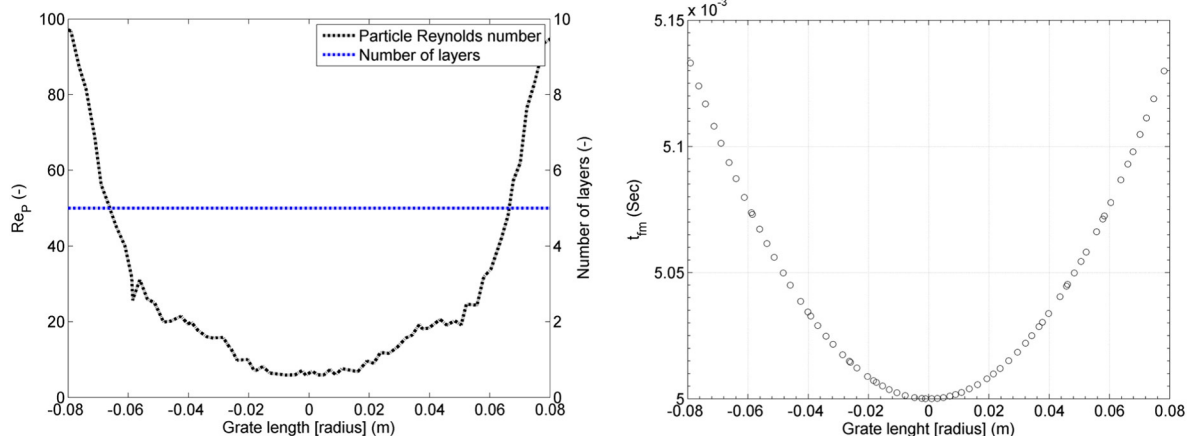


Fig. 11. Particle Reynolds number (–) and number of particle layers (–) (left) as well as estimated mixing time (s) interpolated from calculation points of Fig. 10 (right).

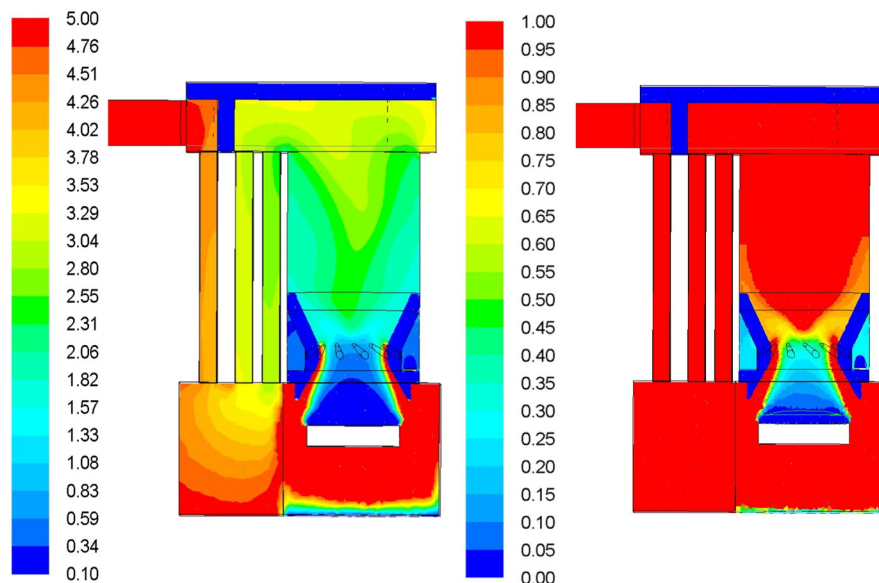


Fig. 12. Gas residence time (s) (left), and mixing function (-) (right) evaluated for wood pellets as fuel.

mixing function is non-uniform, especially, above the grate up to the secondary air nozzles.

Flue gas temperature and O_2 concentrations calculated with all models for both wood pellets (top) and straw pellets (bottom) are shown in Figs. 13 and 14, respectively. The simulations show for both cases low O_2 concentrations (see Fig. 14) and high flue gas temperatures (see Fig. 13) in the major reaction zone above the fuel bed in the primary combustion zone as well as close to the secondary air injection. Here, also the peak flue gas temperatures can be observed.

The regions addressed correspond to increased combustion progress which is more pronounced in the case of EDC and hybrid simulations than in the case of the EDM simulation. The higher flue gas temperatures predicted with the EDC compared to the EDM are attributed to the Magnussen constant of the EDM model [8] which is systematically adapted for biomass grate furnaces by a comparison with CO emission

and temperature measurements [11,14]. Accordingly, a reduction of the mixing and the reaction rate compared to the original model is achieved. Therefore, the EDC, where no tuning is done, predicts higher reaction rates, which rise the temperatures. The higher temperatures predicted with the hybrid model compared to the EDC are pertaining to influence of the combustion models (e.g. FRK or EDC model) in the hybrid model which depend on the local turbulent Reynolds number of the flow. Hence, it is of interest to investigate the flow regime in the combustion chamber. Fig. 15 shows the flue gas temperatures and the turbulent Reynolds number obtained with different gas phase reaction models for wood pellets as fuel. The figure shows that the turbulent Reynolds number is lower than 64 in the major reaction zones that are indicated by high temperature zones above the fuel bed at the outer edge of the grate as well as close to secondary air injection and, therefore, the reaction rate in the hybrid model is calculated mostly with the FRK model in these regions.

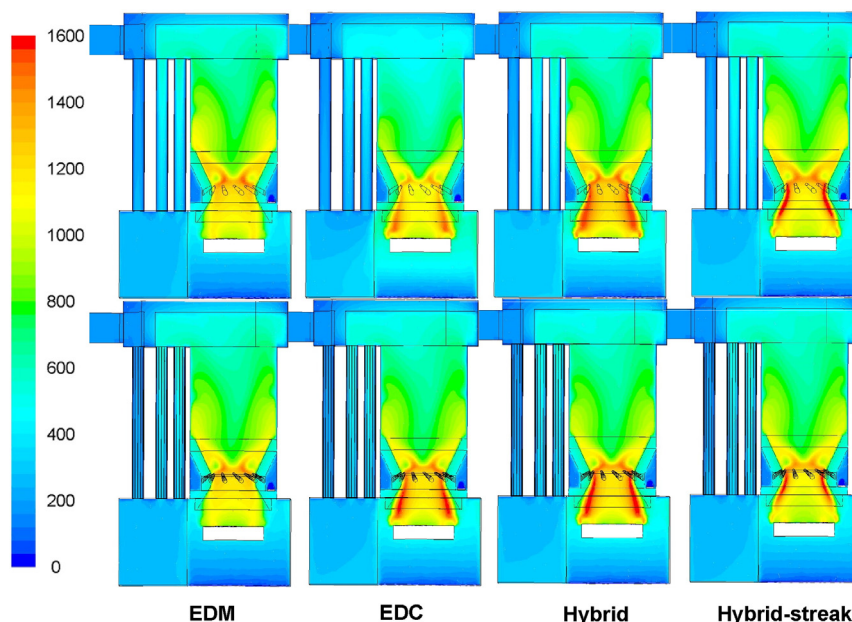


Fig. 13. Iso-surfaces of flue gas temperatures ($^{\circ}C$) in a vertical cross-section of the furnace for wood pellets (top) and straw pellets (bottom).

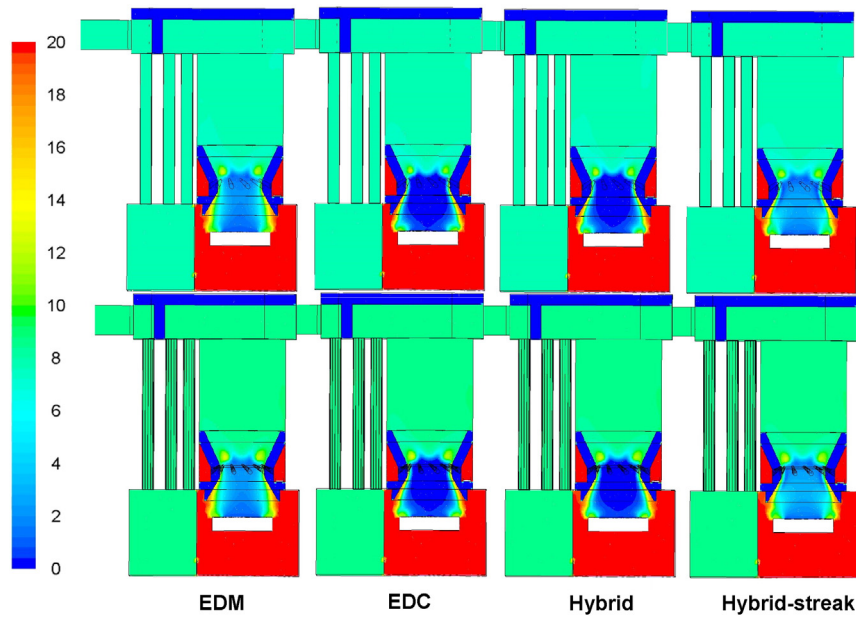


Fig. 14. Iso-surfaces of O₂ concentrations (vol.% dry) in a vertical cross-section of the furnace for wood pellets (top) and straw pellets (bottom).

The flue gas temperatures predicted with the hybrid-streak model are somewhat different. It was shown that the major part of the reaction zone above the packed bed is also influenced by streak formation (i.e. the mixing function) (see Fig. 12). It is clear that the combustion progress is slowed down by the hybrid-streak model in the regions where the streaks exist (above the grate). The same trend can be found for the O₂ concentration fields. As can be seen from Fig. 14, the O₂ concentrations calculated with the hybrid-streak model are higher, especially in the primary combustion zone, because the combustion progress is delayed due to a poor mixing caused by the presence of streaks.

Significant differences can also be observed in the prediction of CO concentrations with the EDM, the EDC, the hybrid model and the hybrid-streak model as shown in Fig. 16. Generally, the EDC and hybrid model resulted in a much faster CO oxidation, especially in the regions of intense mixing in the primary combustion zone and in the region directly after the secondary air injection, while the EDM with the mixing parameter applied leads to a generally slower CO oxidation. Therefore,

EDC and hybrid led to significantly lower CO levels further downstream in the secondary combustion zone and at boiler inlet.

Moreover, the slight differences in the CO concentrations between the EDC and the hybrid model are mainly due to a higher reaction rate caused by a higher contribution of the FRK model, where micro-mixing plays no role (see Tables 2 and 3).

The CO prediction with the hybrid-streak model is higher than for the EDC and the hybrid model since the combustion progress is delayed due to the presence of streaks (see Fig. 12) mainly in the primary combustion zone. The predicted CO concentrations at boiler outlet for both wood and straw pellets are given in Tables 2 and 3. For wood pellets (see Table 2), the calculated CO value predicted with the hybrid-streak model is in best agreement with the measured values. The better prediction with the hybrid-streak model can be explained by a delay in the CO oxidation, since the net reaction rate in the hybrid-streak model is multiplied by the mixing function, therefore, the regions above the major flue gas release zone and the reaction fronts are mainly

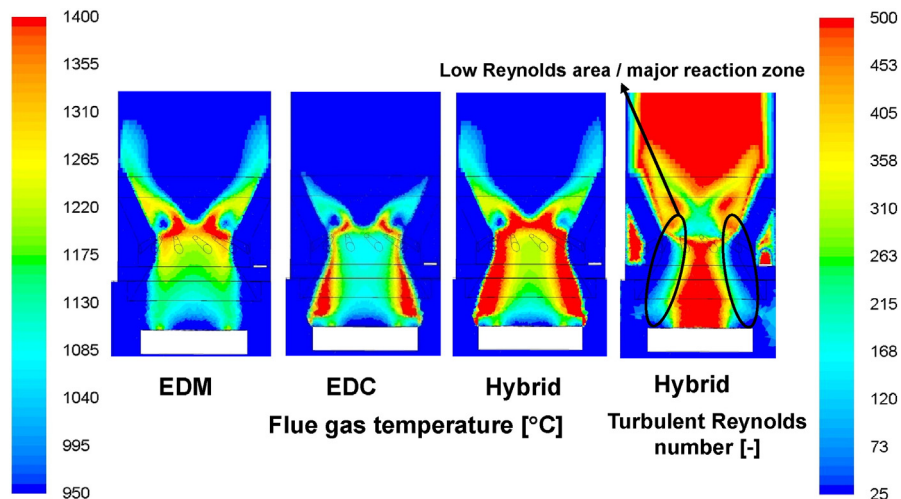


Fig. 15. Iso-surfaces of flue gas temperatures (°C) (left) and turbulent Reynolds number (-) (right) in a vertical cross-section of the furnace (up to the upper edge of the refractory lining) evaluated for wood pellets as fuel.

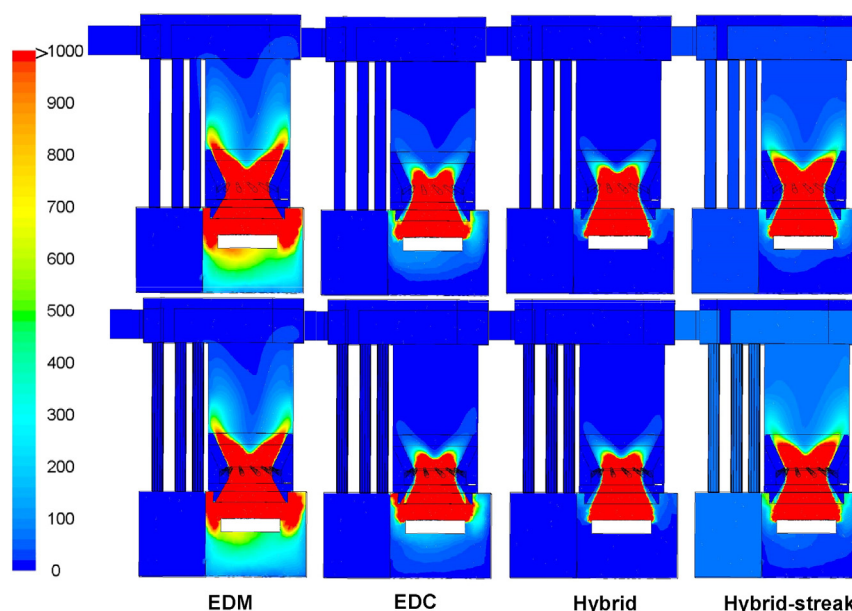


Fig. 16. Iso-surfaces of CO concentrations (ppmv) in a vertical cross-section of the furnace for wood pellets (top) and straw pellets (bottom).

influenced by mixing function. The CO values calculated with the EDC model are in better agreement with measured values than the hybrid and the EDM model. The hybrid model results in a much faster CO oxidation, since the major part of the reaction progress is calculated with the FRK, while in the EDM the reaction rate is mainly controlled by the mixing constant, A_{mag} [8] which is tuned [11,14]. In the case of straw pellets, the CO values predicted with the hybrid-streak model are in better agreement than the EDC and hybrid model due to a more accurate prediction of mixing processes above the packed bed. The CO values predicted with the EDC and hybrid model are too low in comparison with the measured values. The EDM gives the best agreement with the measured CO values. As already explained, the eddy dissipation rate is directly proportional to the value of the modelling constant A_{mag} [8] and to the mean eddy lifetime, k/ε where the value of A_{mag} is lowered from the originally proposed value, $A_{mag} = 4$, to $A_{mag} = 0.8$ for the simulation of small scale biomass combustion plants [11,14]. Besides, there is no explicit modelling of streaks with the EDM model and the model is valid for highly turbulent flows which mean that the best agreement in this case is due to good tuning for grate combustion plants but a model which can predict reliable CO burnout rates without tuning would be preferable. A clear drawback of the EDM in combination with global reaction mechanisms is that it is not able to describe complex interactions of turbulence and multi-step reaction kinetics. Besides, when modelling gas phase combustion with the EDM basically we are already tuning the model constant A_{mag} by nearly an order of magnitude. This is actually not satisfactory since tuning of model constants over such a wide range may lead to a limited validity range linked with wrong predictions under deviating conditions (e.g. the effect of mixing may be overestimated especially in kinetically limited zones). In order to

avoid this, the EDC and the Hybrid model, which provide a more fundamental prediction of gas phase reactions, have been applied. However, they are more sensitive to the boundary conditions at the surface of the fuel bed (turbulence and mixing degree) and hence need an additional model, which explicitly considers the effects of streaks on the mixing. By introducing this model, no tuning of the gas phase combustion model to fixed bed combustion is necessary.

The characteristics of reacting radicals (e.g. OH and O) are important for an in-depth understanding of the combustion and NO_x formation processes [14]. These radicals are of high relevance especially for the formation of NO_x . The OH and O species calculated with the EDC, hybrid and hybrid-streak model for straw pellets are shown in Fig. 17. The OH and O species are generally predicted highest with the hybrid-streak model since the rates of production or destruction of the species are slowed down due to multiplication of the mixing function (see Eq. (18)).

As known from already performed research [24,25], NO_x formation in fixed bed biomass combustion plants is dominated by fuel NO_x . Moreover, NO is the clearly dominating species formed [25].

As already mentioned, a skeletal reaction mechanism (28 species and 102 reactions in total) was applied [15] for the simulation of NO_x formation, and the simulation was performed in a post-processing step.

Experimental data of the combustion and release behaviour for a variety of solid biomass fuels have been gained through several measurement campaigns in a lab-scale packed bed pot furnace reactor [24,25]. These experimental data include the concentration profiles of the N containing species NO, NH_3 , HCN, NO_2 and N_2O released from the fuel bed over time. The measured profiles are utilised for the derivation of release functions for the most relevant NO_x precursors measured. The

Table 2

Predicted CO concentrations with the EDM, EDC, hybrid and hybrid-streak models in comparison to measurements for wood pellets.

Average CO concentration	Unit	Simulations				Measurement
		EDM	EDC	Hybrid	Hybrid-streak	
Boiler outlet	[ppm dry]	16	19	5	30	38
Boiler outlet	[mg/Nm ³ 13 vol.% O ₂ dry]	10	15	3	22	29
Deviation (percent error)	[%]	-65	-48	-89	-24	

Table 3

Predicted CO concentrations with the EDM, EDC, hybrid and hybrid-streak models in comparison to measurements for straw pellets.

Average CO concentration	Unit	Simulations				Measurement
		EDM	EDC	Hybrid	Hybrid-streak	
Boiler outlet	[ppm dry]	13	4	3	29	16
Boiler outlet	[mg/Nm ³ 13 vol.% O ₂ dry]	10	3	2	27	13
Deviation (percent error)	[%]	-23	-76	-84	107	

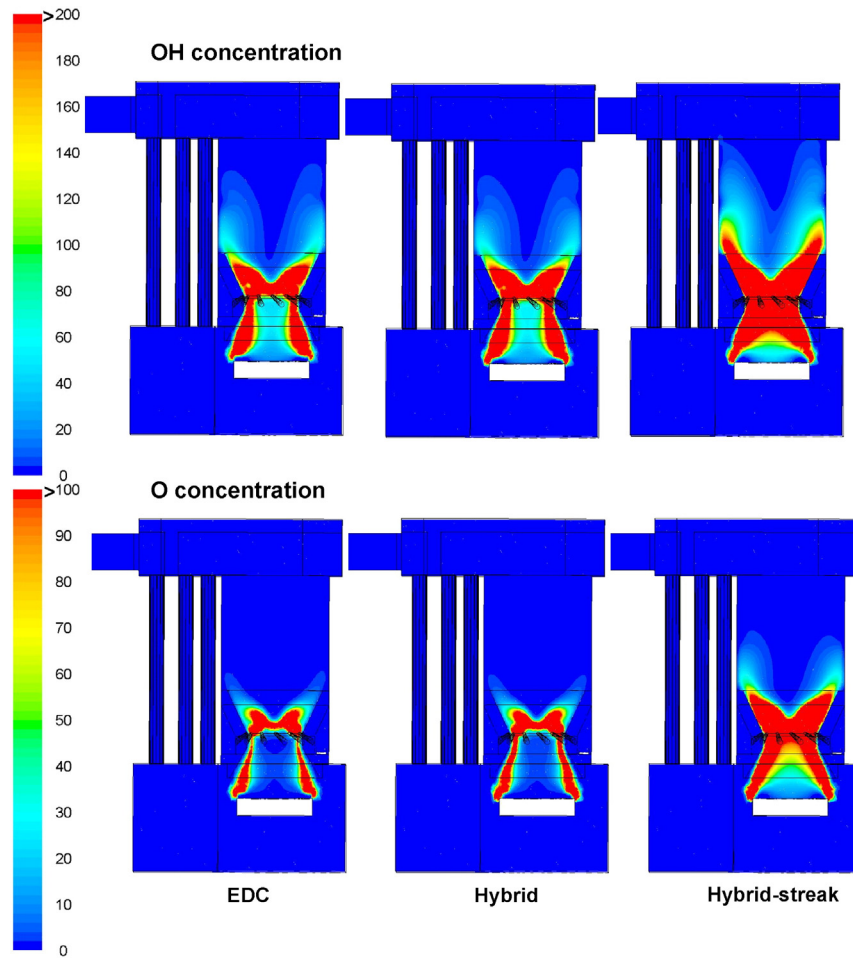


Fig. 17. Iso-surfaces of OH concentration (ppmv dry) (top) and O concentration (ppmv dry) (bottom) for straw pellets in a vertical cross-section of the furnace.

release functions of fuel nitrogen depend on the local air ratio (λ), the nitrogen content of the fuel as well as the N binding in the fuel (the kind of biomass fuel). The most important NO_x precursor detected above the fuel bed for wood (spruce) and straw pellets under fuel rich conditions is NH_3 , while HCN is almost insignificant. NO is detected mainly under air rich conditions (charcoal burnout) [25]. Furthermore,

the experimental data are utilised to derive release functions for the relevant NO_x precursors NO, NH_3 and HCN. The release functions were implemented in an in-house developed empirical packed bed combustion model [24,25], which serves as a basis for the subsequent CFD gas phase simulation of N species conversion. Figs. 18 and 19 show the NO, NH_3 and HCN profiles calculated with the EDC, hybrid and the hybrid-

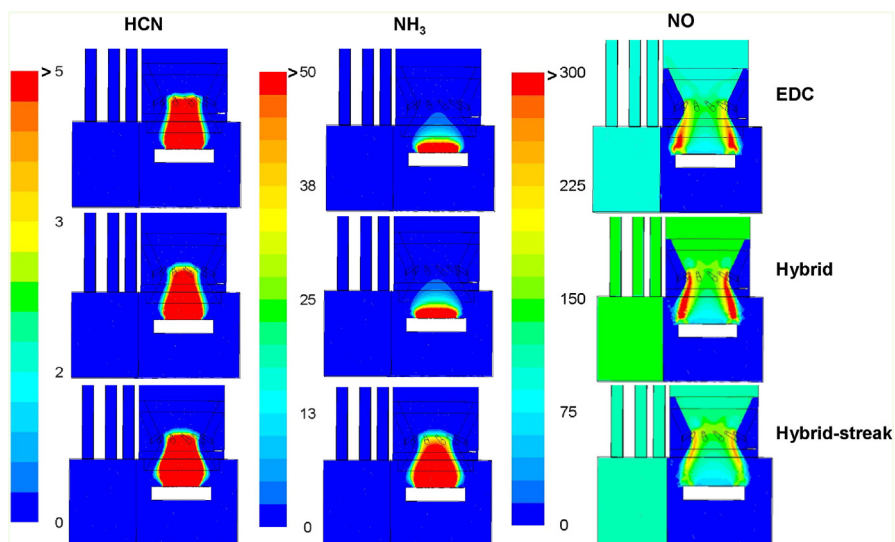


Fig. 18. Iso-surfaces of HCN concentrations (ppmv) (left), NH_3 concentrations (ppmv) (middle) and NO concentrations (ppmv) (right) calculated with the EDC model (top), the hybrid model (middle) and the hybrid-streak model (bottom) for wood pellets.

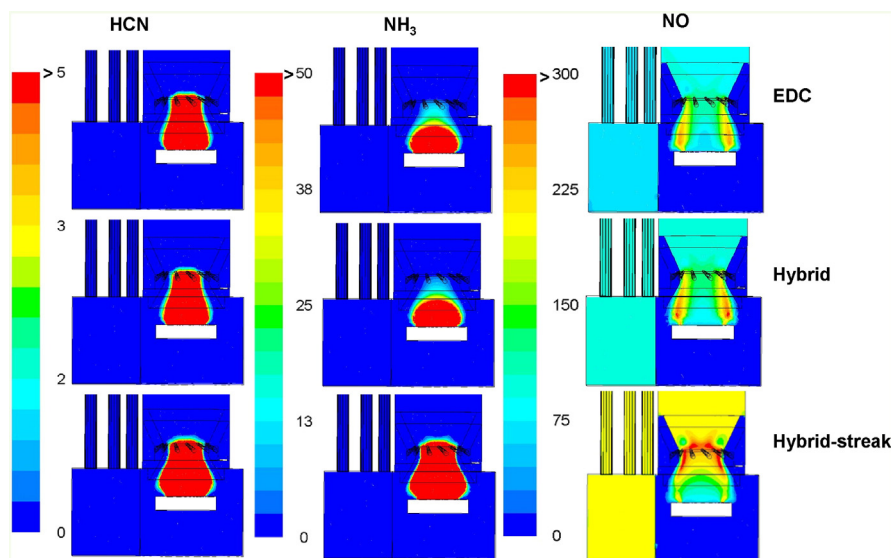


Fig. 19. Iso-surfaces of HCN concentrations (ppmv) (left), NH_3 concentrations (ppmv) (middle) and NO concentrations (ppmv) (right) calculated with the EDC model (top), the hybrid model (middle) and the hybrid-streak model (bottom) for straw pellets.

streak model for wood pellets and straw pellets, respectively. Generally, distinct areas can be observed, where the release of NO, HCN and NH_3 takes place. NO is released in the air-rich zone towards the outer edge of the grate. NO is formed in regions where high temperatures and high concentrations of O and OH radicals prevail [26,27]. The locations, where the NO has been released are co-located with high concentrations of O and OH radicals above the bed (see Fig. 17 for straw pellets). In contrast, NH_3 and HCN are primarily released from the main in-bed devolatilisation/gasification zone. These differences result from the local differences in the in-bed availability of the oxidiser (see Fig. 14), which in turn depends on the amount and distribution of primary air under the grate as well as on the in-bed thermal conversion processes. The distribution of N-containing species in the gas phase results from the simultaneous formation and reduction processes, taking place in different regions of the combustion chamber and depends on many factors.

The regions, where NO reduction takes place in the combustion chamber, can be observed by looking at reaction $\text{N}_2 + \text{O} \rightleftharpoons \text{NO} + \text{N}$

[14] (NO reduction) as shown in Figs. 20 and 21 for both wood pellets and straw pellets. Generally, NO released from the fuel bed as well as locally formed in the gas phase is primarily consumed in the primary combustion zone (see Fig. 13, O_2 distribution). Here, products of NH_3 (and HCN) breakdown act as reducing agents, as can be seen by comparing profiles of NO, NH_3 and HCN (see Figs. 18 and 19) and the kinetic reaction rate of N_2 (see Figs. 20 and 21 (left)). The regions of high NH_3 concentrations and low availability of O_2 overlap with the regions of an increased NO reduction. Simultaneously, NO is locally produced in the primary combustion zone in the outer grate zones, above the fuel bed, as well as in front of the secondary air jets at the oxygen rich side of the flame (see Fig. 13). Processes related to NO formation and reduction are also relevant close to the area affected by the injection of secondary air.

Generally, the higher NO formation in the case of straw pellets (see Tables 4 and 5), especially in the primary combustion zone, is mainly attributed to the higher fuel nitrogen content (approximately seven times higher than wood pellets) (see Table 1). Fig. 22 shows the NO_x

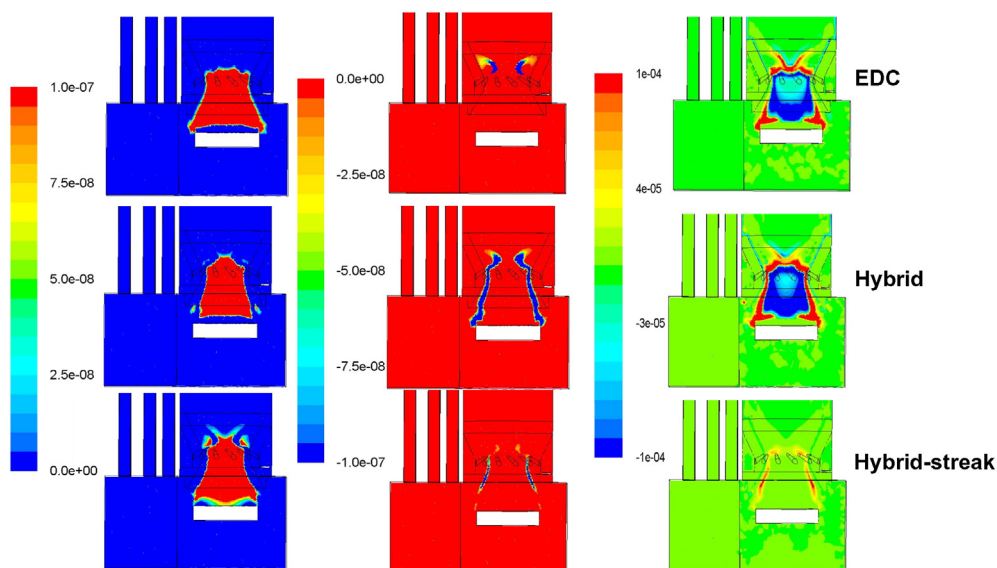


Fig. 20. Iso-surfaces of reaction rates for the reaction $\text{N} + \text{NO} \rightarrow \text{N}_2 + \text{O}$ (reduction to N_2) ($\text{kmol}/(\text{m}^3 \text{ s})$) (left), for the reaction $\text{N}_2 + \text{O} \rightarrow \text{N} + \text{NO}$ (NO formation from N_2) ($\text{kmol}/(\text{m}^3 \text{ s})$) (middle) and for the net reaction rate of NO formation ($\text{kg}/(\text{m}^3 \text{ s})$) (right) calculated with the EDC model (top), the hybrid model (middle) and the hybrid-streak model (bottom) for wood pellets as fuel.

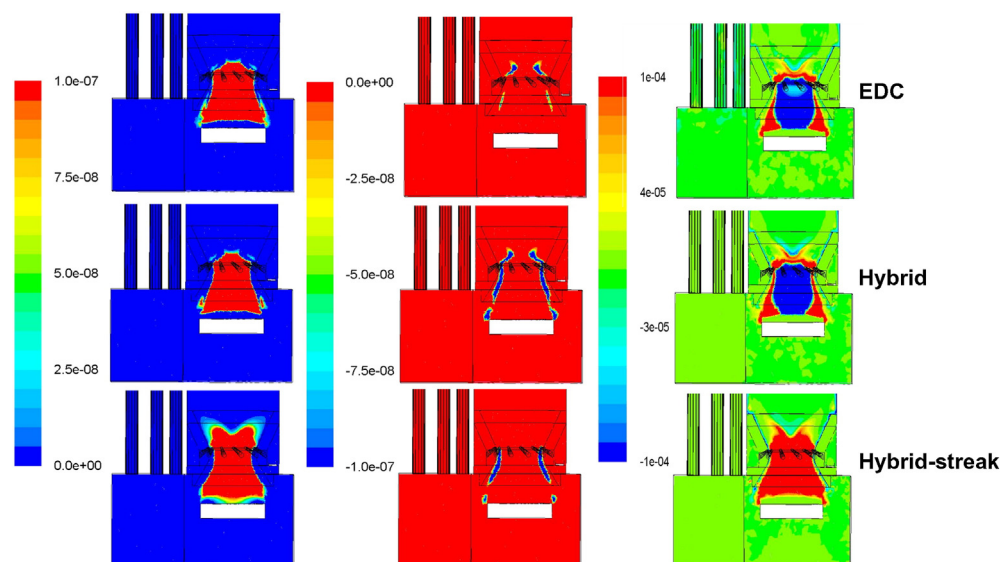


Fig. 21. Iso-surfaces of reaction rates for the reaction $N + NO \rightarrow N_2 + O$ (reduction to N_2) ($\text{kmol}/(\text{m}^3 \text{ s})$) (left), for the reaction $N_2 + O \rightarrow N + NO$ (NO formation from N_2) ($\text{kmol}/(\text{m}^3 \text{ s})$) (middle) and for the net reaction rate of NO formation ($\text{kg}/(\text{m}^3 \text{ s})$) (right) calculated with the EDC model (top), the hybrid model (middle) and the hybrid-streak model (bottom) for straw pellets as fuel.

emissions in dependence of the fuel nitrogen content for different biomass fuels. The experimental data are from different plants fired with different fuels [28,29]. The intention is to show the trends of NO_x emissions in dependence of different biomass fuels used with varying fuel nitrogen contents and to check if the simulated values predicted are in the correct range. The simulation results (NO_x simulation with the hybrid-streak model) are also provided in the figure. The results indicate that a higher N content of the fuel leads to higher NO_x emissions in the gas phase during the combustion process.

The simulation results with the EDC, the hybrid and the hybrid-streak model show substantial differences in terms of NO_x profiles for wood pellets and straw pellets. Fig. 23 shows the NO_x profiles predicted with the different models for wood pellets (top) and straw pellets (bottom). The predicted NO_x concentrations at boiler outlet for both wood pellets and straw pellets are given in Tables 4 and 5. According to the hybrid model, the major part of the reaction zones is located above the grate as well as in front of the secondary air jets, where the turbulent Reynolds number is lower than 64. Therefore, the reaction progress is mainly calculated with the FRK model, whereas micro-mixing plays no important role. This causes a higher net reaction rate of NO in these regions (see Figs. 20 and 21 (middle)). However, in the EDC, the reaction progress is always influenced by micro-mixing. According to this model, the fluid is in any case mixed on a micro-scale and the reactions finally take place in the fine structures [9] of the fluid, where the reactants are mixed on a molecular level. Hence, the EDC fails to predict reactive flows in laminar and moderately turbulent situations. Therefore, in this case, the EDC leads to a higher NO_x reduction, since NO_x formation in the outer air-rich zone in the primary combustion zone is stronger decreased than the NO_x reduction in the air lean zone of the

primary combustion zone (see Tables 4 and 5). Furthermore, the NO_x formation processes according to the hybrid-streak model are completely different from the EDC and the hybrid model.

Here, it can be seen that the spatial distributions of NO, NH_3 and HCN are different especially above the fuel bed (see Figs. 18 and 19). These differences are mainly attributed to the different oxygen and radical (O and OH) concentrations that are influenced by streak formation (i.e. mixing function).

The results for both cases show that the predictions are improved with the hybrid-streak model. This can be explained with the more accurate prediction of the species mixing process above the fuel bed and, therefore, of the radicals, that are important for NO_x formation processes. This means that in the case for straw pellets with a high fuel nitrogen content, where the NO_x formation is dominated by the reaction progress in the reduction zone, which is slowed down by the mixing function since it is multiplied by the net reaction rate in the hybrid-streak model, higher NO_x emissions are predicted than with the other models. For wood pellets with a very low nitrogen content and hence a low concentration of the NO_x reducing agent NH_3 , the overall NO_x reaction progress is dominated by the NO_x formation in the air rich zone of the primary combustion zone, which is again slowed down by the presence of streaks, leading to lower NO_x emissions than for the other models.

4. Summary and conclusions

A streak formation model has been developed to account for the effects of gas streaks arising from the fuel bed of grate combustion plants on gas mixing and reactions. The streak formation model is based on a correlation between the local gas residence time and a mixing time in

Table 4

Predicted NO_x concentrations with the EDC, hybrid and hybrid-streak models in comparison to measurements for wood pellets as fuel.

Average NO_x concentration	Unit	Simulations			Measurement
		EDC	Hybrid	Hybrid-streak	
Boiler outlet	[ppm dry]	118	132	110	105
Boiler outlet	[mg/Nm^3 13 vol.% O_2 dry]	146	165	135	130
Deviation (percent error)	[%]	12	26	5	

Table 5

Predicted NO_x concentrations with the EDC, hybrid and hybrid-streak models in comparison to measurements for straw pellets as fuel.

Average NO_x concentration	Unit	Simulations			Measurement
		EDC	Hybrid	Hybrid-streak	
Boiler outlet	[ppm dry]	167	186	352	286
Boiler outlet	[mg/Nm^3 13 vol.% O_2 dry]	220	247	466	380
Deviation (percent error)	[%]	-41	-34	23	

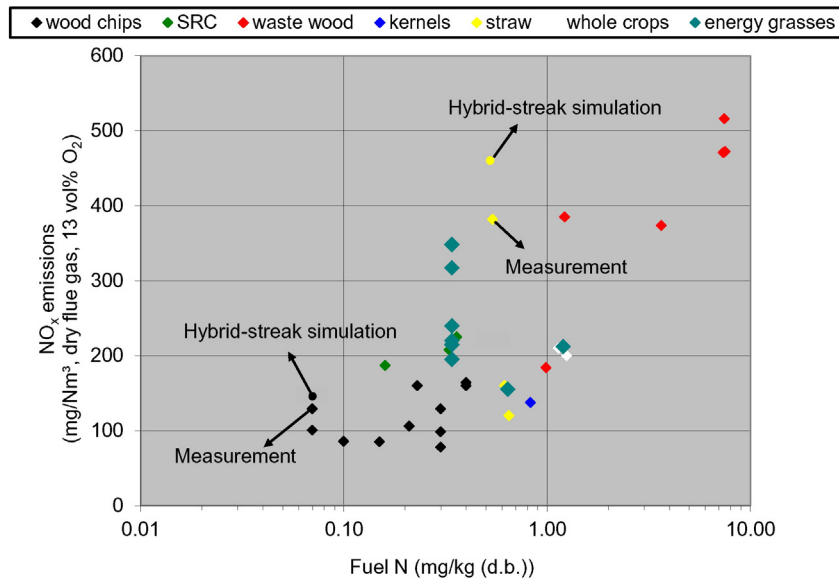


Fig. 22. NO_x emissions in dependence of the fuel nitrogen content for different biomass fuels [25,28,29]. Explanations: SRC: short rotation coppice.

which the mixing time is the necessary time to reach the fully mixed condition in the flue gas. A mixing state definition is introduced in order to evaluate the degree of mixing above the packed bed. The gas residence time introduced in the streak formation model is obtained by solving a scalar transport equation. A series of packed bed CFD case

study simulations has been carried out to derive the mixing time to be considered in the streak formation model. The primary air velocity, volatile mass flow rate and number of particles (bed thickness) were identified as influencing parameters for the derivation of the mixing time. The results of the CFD packed bed case study serves as look-up table

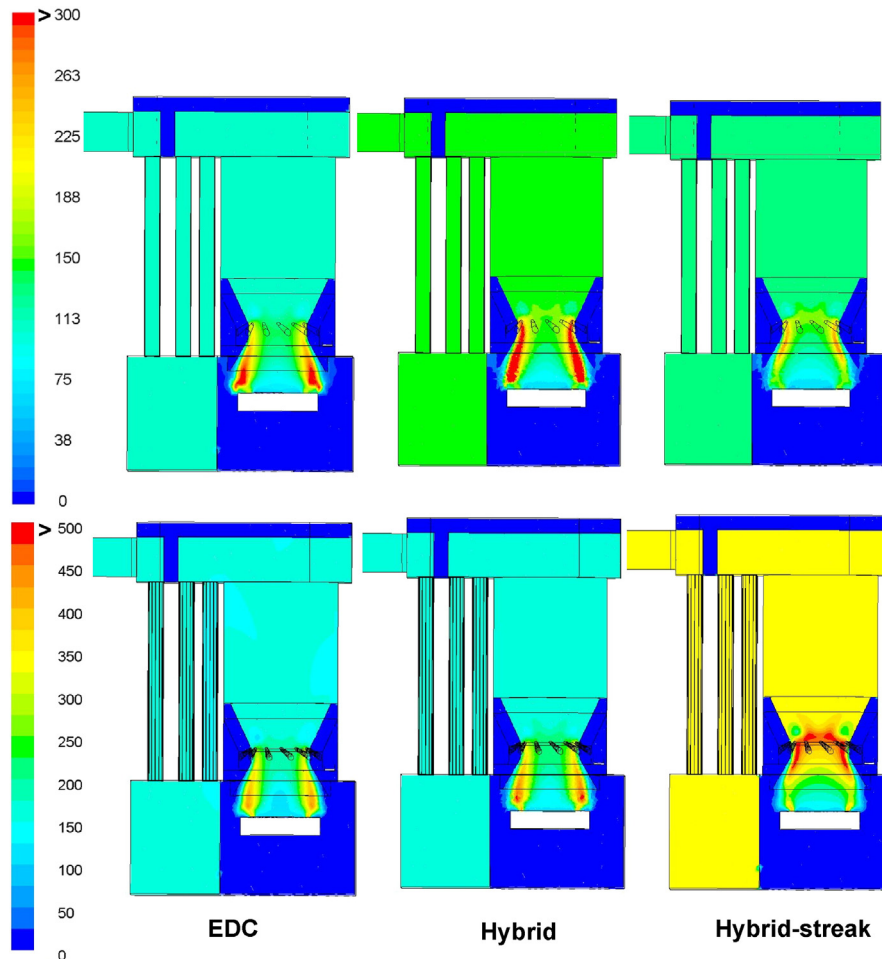


Fig. 23. Iso-surfaces of NO_x concentrations (ppmv dry) in a vertical cross-section of the furnace for wood pellets (top) and straw pellets (bottom).

for the calculation of the mixing time in dependence of the different influencing parameters. The mixing time can be retrieved by a linear interpolation between the calculation points in dependence of the particle Reynolds number and the number of fuel layers. Furthermore, the application of the streak formation model has been verified for an under-feed stoker grate furnace for wood and straw pellets.

The EDM, EDC and hybrid gas phase reaction models are used for the simulation of turbulent reactive flow in the combustion chamber. In the case of the hybrid model, an additional simulation has been performed where, the hybrid and streak formation model have been coupled.

The results from the under-feed stoker case studies show that for both fuels investigated, the streaks have relevant influence on the combustion process regarding flue gas temperature, O_2 distribution and CO emissions. Moreover, the formation of reacting radicals (e.g. O and OH), especially, in the region above the bed are influenced by streak formation since the reaction progress is delayed caused by the incomplete mixing.

In a next step, NO_x simulations have been performed in a post-processing approach based on the solution obtained from the combustion simulations. The distribution of the NH_3 , HCN and NO profiles shows that streak formation has a strong influence on the spatial distributions of the aforementioned species. This is mainly due to the slow-down of the reaction rate predictions caused by the streaks. The NO_x emissions calculated with the hybrid-streak model show the best agreement with measured values. In conclusion, the streak formation model in combination with the hybrid gas phase combustion model shows a clear potential for an improved NO_x prediction since it considers species mixing and reaction processes above the fuel bed with a higher accuracy. In the future, extensive validation simulations for real-scale plants are foreseen in order to validate and evaluate the model in more detail and for different framework conditions.

References

- R. Scharler, Entwicklung und Optimierung von Biomasse-Rostfeuerungen durch CFD-Analyse (PhD Thesis) Graz University of Technology, 2001.
- R. Scharler, E. Widmann, I. Obernberger, CFD modeling of NO_x formation in biomass grate furnaces with detailed chemistry, in: A.V. Bridgwater, D.G.B. Boocock (Eds.), Science in Thermal and Chemical Biomass Conversion; Sept 2004, CPL Press, Victoria, Canada; UK 2006, pp. 284–300.
- A. Shiehnejadhesar, K. Schulze, R. Scharler, I. Obernberger, A new innovative CFD-based optimisation method for biomass combustion plants, Biomass Bioenergy 53 (2013) 48–53.
- ÖNORM M 7135, Compressed Wood or Compressed Bark in Natural State, Pellets and Briquettes. Requirements and Test Specifications, Österreichisches, Vienna, Austria, 2003.
- A. García-Maraver, V. Popov, M. Zamorano, A review of European standards for pellet quality, Renew. Energy 36 (2011) 3537–3540.
- R. Mehrabian, S. Zahirovic, R. Scharler, I. Obernberger, S. Kleditzsch, et al., A CFD model for thermal conversion of thermally thick biomass particles, Fuel Process. Technol. 95 (2012) 96–108.
- A. Shiehnejadhesar, R. Mehrabian, R. Scharler, G.M. Goldin, I. Obernberger, Development of a gas phase combustion model suitable for low and high turbulence conditions, Fuel 126 (2014) 177–187.
- B.F. Magnussen, B.H. Hjertager, On mathematical modeling of turbulent combustion with special emphasis on soot formation and combustion, Proc. Combust. Inst. 16 (1) (1977) 719–729, [http://dx.doi.org/10.1016/S0082-0784\(77\)80366-4](http://dx.doi.org/10.1016/S0082-0784(77)80366-4).
- B.F. Magnussen, On the structure of turbulence and a generalized eddy dissipation concept for chemical reaction in turbulent flow, 19th AIAA Aerospace Science Meeting, St Louis, Missouri, USA, 1981.
- A. Brink, Eddy Break-up Based Models for Industrial Diffusion Flames With Complex Gas Phase Chemistry (PhD Thesis) Abo Akademi University, 1998.
- R. Scharler, T. Fleckl, I. Obernberger, Modification of a Magnussen Constant of the eddy dissipation model for biomass grate furnaces by means of hot gas in-situ FT-IR absorption spectroscopy, Prog. Comput. Fluid Dyn. Int. J. 3 (2003) 102–111.
- S.B. Pope, Computationally efficient implementation of combustion chemistry using in situ adaptive tabulation, Combust. Theory Model. 1 (1997) 41–63.
- B. Kader, Temperature and concentration profiles in fully turbulent boundary layers, Int. J. Heat Mass Transfer 24 (9) (1981) 1541–1544.
- S. Zahirovic, R. Scharler, P. Kilpinen, I. Obernberger, Validation of flow simulation and gas combustion sub-models for the CFD-based prediction of NO_x formation in biomass grate furnaces, Combust. Theory Model. 15 (1) (2011) 61–87.
- S. Zahirovic, R. Scharler, P. Kilpinen, I. Obernberger, A kinetic study on the potential of a hybrid reaction mechanism for prediction of NO_x formation in biomass grate furnaces, Combust. Theory Model. 15 (5) (2011) 645–670.
- S.B. Pope, Turbulent Flow, Cambridge University Press, Cambridge, UK, 2001.
- J. Kim, P. Monin, R. Moser, Turbulence statistics in fully developed channel flow at low Reynolds number, J. Fluid Mech. 177 (1987) 133–166.
- M. Bartak, M. Cermak, J.A. Clarke, J. Denev, F. Drkal, et al., Experimental and numerical study of local mean age-of-air, Proc. 7th International Building performance Simulation Association Conference, IBPSA, ISBN: 85-901939-3-4, 2001.
- D.A. Egarr, M.G. Faram, T. O'Doherty, D.A. Phipps, N. Syred, Computational fluid dynamic prediction of the residence time distribution of a prototype hydrodynamic vortex separator operating with a base flow component, Proc. Inst. Mech. Eng. E J. Process Mech. Eng. 219 (1) (2005) 53–67.
- D. Neves, H. Thunman, A. Matos, L. Tarelho, A. Gomez-Barea, Characterization and prediction of biomass pyrolysis products, Prog. Energy Combust. Sci. 37 (2011) 611–630.
- M.L. Boroson, J.B. Howard, J.P. Longwell, W.A. Peters, Product yields and kinetics from the vapor phase cracking of wood pyrolysis tars, AIChE J. 35 (1989) 120–128.
- R.G. Graham, M.A. Bergougnou, R.P. Overend, Fast pyrolysis of biomass, J. Anal. Appl. Pyrol. 6 (1984) 95–135.
- S. Hamel, On the Packing Properties of Fixed Beds for Thermal Fuel Conversion, Shaker Verlag, Germany, 2010. 74–75.
- I. Obernberger, E. Widmann, R. Scharler Entwicklung eines Abbrandmodells und eines NO_x -Postprozessors zur Verbesserung der CFD-Simulation von Biomasse-Festbettfeuerungen, Report from energy and environment research, report No. 31/2003, Ministry for Transport, Innovative and Technology (Ed.), Vienna, Austria.
- G. Stubenberger, R. Scharler, S. Zahirovic, I. Obernberger, Experimental investigation of nitrogen species release from different solid biomass fuels as a basis for release models, Fuel 87 (6) (2008) 793–806.
- S.R. Turns, Understanding NO_x formation in non-premixed flames: experiments and modeling, Prog. Energy Combust. Sci. 21 (1995) 361–385.
- A. Mardani, S. Tabejamaat, NO_x formation in H_2 - CH_4 blended flame under mild conditions, Combust. Sci. Technol. 184 (7–8) (2012) 995–1010.
- I. Obernberger, Strategy for the application of novel characterization methods for biomass fuels: case study of straw, Energy Fuel 28 (2) (2014) 1041–1052.
- T. Hesch, F. Biedermann, T. Brunner, I. Obernberger, Reduction of NO_x and PM_{10} emissions from automated boilers by advanced air staging, in: M. Faulstich (Ed.), 19th European Biomass Conference & Exhibition, June 2011, Berlin, Germany, ETA-Renewable Energies, Florence, Italy 2011, pp. 874–879.

Nomenclature

- $C_{m,i}$: tracer gas concentration in the fully mixed gas (–)
 $C_{l,i}$: local tracer gas (–)
 D_b : molecular diffusivity ($m^2 s^{-1}$)
 D_t : turbulent diffusivity ($m^2 s^{-1}$)
 d_p : volume diameter (m)
 J_i : diffusion flux of species i ($kg m^{-1} s^{-1}$)
 \dot{m} : mass flow rate ($kg s^{-1}$)
 MS : mixing state (–)
 MF : mixing function (–)
 Re_p : particle Reynolds number (–)
 Re_t : turbulent Reynolds number (–)
 R_p : net rate of production of species i by chemical reaction ($kg m^{-3} s^{-1}$)
 $S_{o,i}$: source term ($kg m^{-3}$)
 Sc_i : Schmidt number (–)
 t : residence time (s)
 Δt : time step (s)
 u : fluid velocity ($m s^{-1}$)
 UDF : user-defined function
 UDS : user-defined scalar
 V : volume (m^3)
 V : volumetric flow rate ($m^3 s^{-1}$)
 Y_i : mass fraction of species i (–)

Greek symbols

- ϵ : turbulent dissipation rate ($m^2 s^{-3}$)
 ν : kinematic viscosity ($m^2 s^{-1}$)
 ρ : density ($kg m^{-3}$)
 \vec{v} : velocity vector ($m s^{-1}$)
 φ_k : scalar quantity (residence time) (s)
 Γ_k : diffusion coefficient ($m^2 s^{-1}$)
 μ_t : turbulent viscosity ($kg m^{-1} s^{-1}$)
 μ_l : laminar viscosity ($kg m^{-1} s^{-1}$)

Subscript

- EDC: eddy dissipation concept
FRK: finite rate kinetics
i: species index
t: turbulent